Ann. Geophys., 27, 1343–1352, 2009
www.ann-geophys.net/27/1343/2009/

Annales Geophysicae

Dipole tilt effects in plasma sheet B_y: statistical model and extreme values

A. A. Petrukovich

Space Research Institute, 84/32 Profsoyuznaya st., Moscow, 117997, Russia

Received: 13 October 2008 – Revised: 24 February 2009 – Accepted: 24 February 2009 – Published: 31 March 2009

Abstract. With 11 years of Geotail measurements we construct a model of plasma sheet B_y, depending on IMF B_y, coordinates X, Y, and geodipole tilt angle. At midnight and pre-midnight local times B_y is positively correlated with tilt (positive in summer). Thus in summer B_y is shifted towards positive values and in winter towards negative values, so that up to several nT could be added to the IMF influence. The dawn side plasma sheet B_y generally does not exhibit any tilt dependence, but within 15 R_E the weaker negative correlation with tilt was revealed. The tilt dependence is just a useful parametrization and several mechanisms actually affecting plasma sheet B_y were previously suggested. In particular, similar coupling between tilt and IMF B_y was earlier found in the ionospheric convection patterns. Besides this average response, extreme B_y ($|B_y|>5$ nT, $B_y>$IMF B_y) were often observed (up to 20–25% of cases during solar maximum and in the pre-midnight sector within 20 R_E). They can not be explained by our statistical model and are preliminary interpreted as an "over-reaction" of the magnetosphere in some individual events. Large B_y field radically changes dynamics of the current sheet and has to be taken into account during substorm-related studies.

Keywords. Magnetospheric physics (Magnetotail; Plasma sheet)

1 Introduction

Magnetic field component B_y appears in the magnetotail due to a number of reasons (GSM frame of reference is used hereafter). The field line flaring creates B_y proportional to local B_x, while the neutral sheet twist creates B_y proportional to local B_z (e.g., Fairfield, 1979; Tsurutani et al., 1984; Kaymaz et al., 1994a; Kullen and Janhunen, 2004). These two effects could be corrected with some further adjustment of the proper reference frame and do not alter principally the geometry, since the cross-tail current remains perpendicular to the magnetic field. Regular magnetotail B_y other than that is usually described in terms of penetration of IMF B_y (hereafter B_y^i) (e.g., Cowley and Hughes, 1983). It should be noted however, that physical mechanisms actually responsible for appearance of the IMF-related B_y may be rather complicated. Therefore the term "penetration" is not rigorously justified, though it is frequently used in a rather broad sense as a measure of proportionality between IMF and plasma sheet field. Statistically determined penetration efficiency varies from 0.1 to 0.8 (see a review in Kaymaz et al., 1994b). In the lobes it is small ∼0.1–0.15, while in the plasma sheet it increases towards Earth from ∼0.2 in the distant tail to ∼0.6 in the ISEE-1,2 data set (Sergeev, 1987) and to ∼0.8 at the GOES orbit (Wing et al., 1995). IMF-related B_y is parallel to the (horizontal) cross-tail current and thus the tail magnetic structure becomes essentially three-dimensional.

Physics of B_y formation in the plasma sheet is generally related with the magnetospheric dynamics. Cowley (1981) suggested that IMF B_y induces asymmetries in the tail adding reconnected flux preferentially to different sides of northern and southern lobes (see also Birn, 1990). Asymmetric convection cells in the opposite hemispheres may move the ionospheric ends of the field lines differently, thus tilt the lines and drive additional increase of B_y in the plasma sheet (Moses et al., 1985; Voigt and Hilmer, 1987). It was also suggested that Earthward plasma sheet convection may be responsible for enhancement of B_y (Hau and Erickson, 1995). Distribution of B_y across the tail is therefore interpreted in terms of two components, a smaller one filling the whole tail, and a larger one induced only in the plasma sheet. Magnetospheric field-aligned currents (region 1) may create more localized B_y in the plasma sheet (Tsyganenko et al.,

Correspondence to: A. A. Petrukovich
(apetruko@iki.rssi.ru)

Published by Copernicus Publications on behalf of the European Geosciences Union.

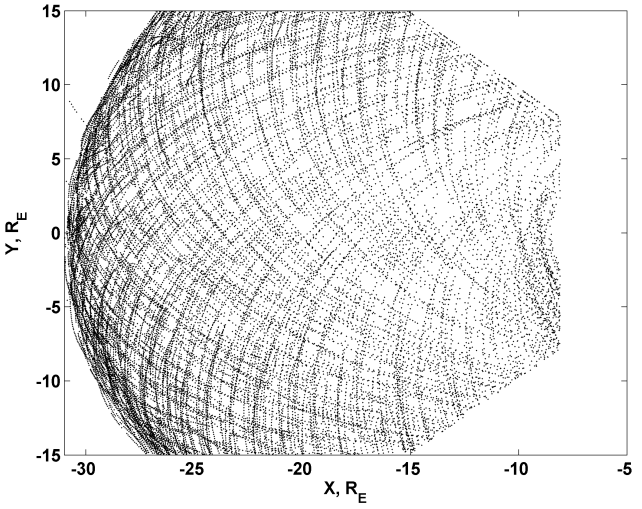

Fig. 1. Coordinates of Geotail observations during 1995–2005 used in the analysis. Each point corresponds to a 15 min interval.

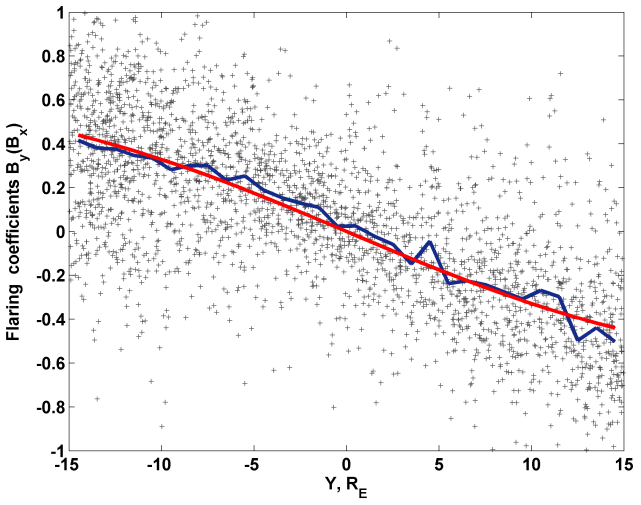

Fig. 2. Grey dots – the linear fit coefficients R of B_y w.r.t. to B_x in 15-min long intervals at $-20\,R_E<X<-18\,R_E$. Blue curve – the box average. Red curve – the approximation with the hyperbolic tangent. See text for details.

1993). Though the effect was not explicitly described, it is actually included in T96 and T01 magnetospheric models (see Sect. 5.2) (Tsyganenko and Stern, 1996).

With such penetration efficiency and average (IMF) $|B_y^i|\sim 3$ nT, plasma sheet B_y is believed to be a minor component, generally smaller than B_z. However, recently in a Cluster project study of the growth phase-related thin current sheets at $-15<X<-20\,R_E$ it was shown that extreme B_y (larger than 5 nT and larger than corresponding IMF B_y) appears in almost 30% of cases (Petrukovich et al., 2007). Large plasma sheet B_y was reported also previously in some event studies (Sergeev et al., 1993; McComas et al., 1986; Nakamura et al., 2008), but this aspect was not addressed in detail so far. Presence of a large current-aligned magnetic component substantially changes particle dynamics, mapping, etc and therefore affects substorm studies in a variety of ways. Several aspects of this problem are discussed in Sect. 5.4. Geotail has by far superior coverage of the magnetotail than any other mission. Therefore we analyze these observations with a specific aim to revisit formation of plasma sheet B_y and to determine occurrence of large B_y.

2 The data and the approach

Geotail magnetic field data (Kokubun et al., 1994) with the 12-s sampling, measured during 1995–2005 in the range $-31<X<-8\,R_E$, $-15<Y<15\,R_E$, $|Y|<|X|$, were used in this investigation. Geotail orbit offers relatively even coverage of this domain (Fig. 1). The flaring-related component of B_y is proportional to B_x and may be quite large at the flanks and for larger B_x. Flaring does not contribute to B_y in the neutral sheet, but selection of only $|B_x|<5$ nT with relatively small flaring effect substantially reduces amount of usable data and hence limits statistical significance of results. There is no ultimate solution to this problem. Making averages between the spatial bins, in a hope that effects of B_x of the opposite signs will cancel each other, may smear out fine details, related with anomalous B_y.

Therefore the following algorithm was designed. All data were sequentially divided in 15-min intervals, containing at least 75% of 12-s samples with $|B_x|<15$ nT. This criterion also selects only the inner (high-β) plasma sheet. In each such interval the linear fit coefficient R defining the flaring effect, $B_y\sim R\cdot B_x$ was determined. R is supposed to depend on Y, but the actual scatter is rather large (Fig. 2) and it was not possible to use these values directly. Instead the model coefficient $R_i^m(X_i, Y)=A_i\tanh(Y/D_i)$ depending on the Y coordinate was set up. The free parameters A_i and D_i were determined during nonlinear fits of R_i^m to R in the set of 2-radii wide bins along the X coordinate (denoted by the subscript i). Only the intervals with the maximum B_x variation larger than 5 nT were used. A sample $R_i^m(Y)$ is shown in Fig. 2 by a red curve. The maximum R_i^m (at the flanks) varies from $\sim$0.2 in the tail-most bin to $\sim$0.7 in the Earth-most bin. Thus we define the model flaring-related $B_y^f=R_i^m(X_i, Y)\cdot B_x$ and subtract it from the measured B_y. All following analysis was performed with such flaring-corrected values.

Finally the data were averaged in each 15-min interval only over the samples with $|B_x|<15$ nT. The final set contains 29 574 of 15-min points. Each such point was augmented with the current and previous (up to 10 h) solar wind and IMF data taken from the 5-min OMNI data set. A number of factors of lesser importance (such as the tail twist or the solar wind aberration) might also affect our analysis. They were not taken into account in the primary model and will be discussed in Sect. 5.1.

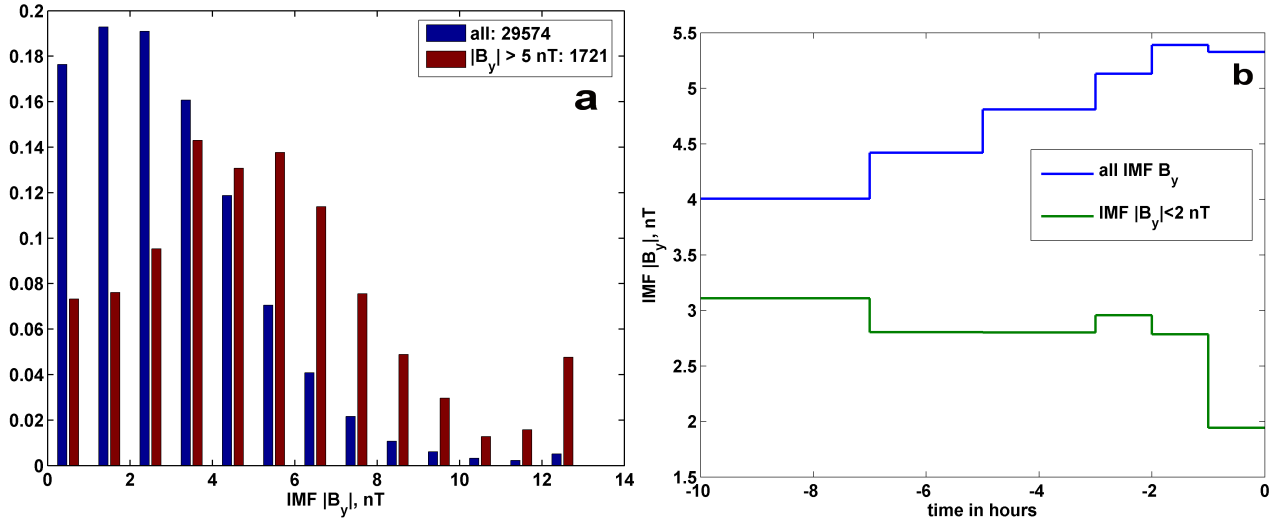

Fig. 3. (a) Histogram of IMF $|B_y|$ for the whole data set and for $|B_y|>5$ nT. **(b)** IMF B_y for 10 h preceding to observation of $|B_y|>5$ nT for all values of IMF B_y (blue) and for only small IMF B_y (green).

Table 1. Occurrence of large By for several data subsets. # – number of points with $|B_y|>5$ nT; percentage of points $|B_y|>5$ nT and $|B_y|>3$ nT; $<|B_y^i|>$ – average IMF in a subset.

Selection	#, $\lvert B_y\rvert>5$ nT	%, $\lvert B_y\rvert>5$ nT	%, $\lvert B_y\rvert>3$ nT	$<\lvert B_y^i\rvert>$, nT
all	1721	5.8%	17%	3.0
$-31<X<-20\ R_E$	600	3.2%	12%	3.0
$-20<X<-10\ R_E$	749	10%	26%	3.1
$-20<X<-10\ R_E$, $-5<Y<10\ R_E$	426	13.3%	31%	3.1
$-20<X<-10\ R_E$, $Y>10\ R_E$, $Y<-5\ R_E$	323	7.7%	22%	3.1
$-20<X<15\ R_E$, $0<Y<10\ R_E$, $B_z<3$ nT, after 2000	39	21%	40%	3.7

3 Occurrence of extreme B_y

In the first place occurrence of large B_y ($|B_y|>5$ nT) was investigated. Table 1 contains the number and the percentage of $|B_y|>5$ nT, the percentage of $|B_y|>3$ nT, the average IMF $|B_y^i|$ for the several spatial subsets. The fraction of $|B_y|>5$ nT was 6% of the full data set, just about 4% at larger downtail distances (20–31 R_E) but it increased up to 13% in the midnight and pre-midnight sector ($-5<Y<10\ R_E$) and closer to Earth ($-20<X<-10\ R_E$). Outside this Y sector the occurrence drops by a factor of two. With the additional selections, bringing the Geotail data closer to the Cluster cases (the last line in Table 1: 15–20 R_E downtail, the thin plasma sheet with the small $B_z<3$ nT and the years after 2000), the percentage became higher than 20%. For $|B_y|>3$ nT then it was almost 40%. Therefore large B_y is indeed quite common in some sectors of the magnetotail and in some conditions.

The last subset (the last line of Table 1) has $<|B_y^i|>\sim 3.7$ nT, higher than that for the whole set (3 nT). Therefore higher IMF, in particular during solar maximum, may contribute to more frequent appearance of large $|B_y|$. In more detail this IMF dependence is analyzed in Fig. 3 and Table 2. Table 2 compares $<|B_y|>$, $<|B_y^i|>$, and $<|B_z^i|>$ for several data subsets. Nominally plasma sheet B_y is expected to be of the order of 40–50% of IMF. Indeed for the full data set IMF B_y is larger than plasma sheet B_y (the first line of Table 2). However, for the selection $|B_y|>5$ nT average IMF $<|B_y^i|>$ was 5.3 nT, that is smaller than the plasma sheet component (the second line of Table 2). The result for $|B_y|>3$ nT was similar. On the other hand the selection of large IMF $|B_y^i|>5$ nT had relatively small $<|B_y|>$ again in agreement with the nominal penetration (the last line of

Table 2. Relation between large B_y and IMF B_y^i, B_z^i.

Selection	$<\lvert B_y\rvert>$, nT	$<\lvert B_y^i\rvert>$, nT	$<B_z^i>$, nT
all	1.8	3.0	0.44
$\lvert B_y\rvert>5$ nT	7.5	5.3	−.01
$\lvert B_y\rvert>3$ nT	5.1	4.3	0.09
$\lvert B_y^i\rvert>5$ nT	3.0	6.8	0.61

Table 3. Occurrence of large B_y (in %) with respect to signs of tilt τ and IMF B_y^i.

Selection	$B_y>5$ nT	$B_y<-5$ nT
$-31<X<-20\ R_E$		
$\tau<0$, $B_y^i<0$	0.1	3.2
$\tau<0$, $B_y^i>0$	1.5	0.3
$\tau>0$, $B_y^i<0$	0.5	1.3
$\tau>0$, $B_y^i>0$	6.2	0.1
$-20<X<-10\ R_E$		
$\tau<0$, $B_y^i<0$	0.5	14.7
$\tau<0$, $B_y^i>0$	7.8	2.7
$\tau>0$, $B_y^i<0$	3.4	6.2
$\tau>0$, $B_y^i>0$	13.4	0.8

Table 2). The average IMF B_z for the large B_y was a bit more negative than for the whole data set, but both B_z^i distributions were similar (not shown here).

Figure 3a shows a histogram of IMF $|B_y^i|$ for $|B_y|>5$ nT and for the whole data set. The maximum of IMF occurrence for the large plasma sheet field is at the moderately large $|B_y^i|$ of the order of 5 nT. Extremely large $|B_y^i|>12$ nT, required by the nominal penetration efficiency, are only ∼5% of observations. The IMF distribution for the whole data set is distinctly different and has no maximum at $|B_y^i|\sim5$ nT.

$|B_y|>5$ nT were not associated with a preceding substantially larger B_y^i. On average IMF B_y^i remained within 5 nT during preceding 10 h (Fig. 3b). Even for the cases with the rather small current IMF $|B_y^i|<2$ nT, the preceding IMF was within 3 nT on average (the green curve in Fig. 3b). Therefore in the most of cases large plasma sheet $|B_y|$ were not related with proportionally larger IMF B_y^i, required by nominal penetration and another explanation is necessary.

One possible factor, contributing to such extreme plasma sheet B_y, is revealed in Table 3, where two spatial subsets from Table 1 are split to positive and negative B_y^i and positive and negative geodipole tilt angle τ. Configurations with the same signs of tilt angle and B_y^i significantly increase probability of appearance of large B_y with the corresponding sign. If tilt and B_y^i signs are opposite, the effect is much weaker, but sometimes the large B_y with the "wrong" sign with respect to IMF was detected. About 50% of such peculiar cases were with $|B_y^i|>3$ nT, so this effect occurs not only when $|B_y^i|$ is close to zero and it's sign is not so important (not shown here). In order to further investigate origins of extreme B_y, one needs a basis, a comprehensive statistical model of B_y, defining an average reaction of the magnetosphere to IMF B_y and other parameters. This is done in the next section.

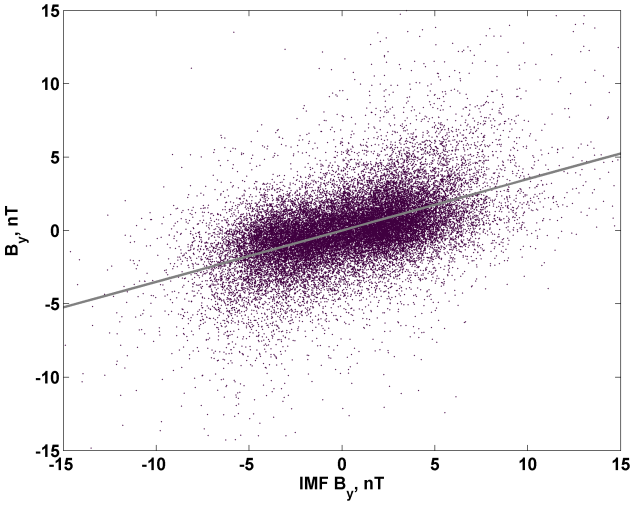

Fig. 4. IMF B_y – plasma sheet B_y scatter-plot. The grey line corresponds to a penetration efficiency of 0.3544.

4 The statistical model of plasma sheet B_y

The main driver of B_y in the plasma sheet is IMF B_y, but their correlation is rather moderate (Fig. 4). The grey solid line in Fig. 4 shows the linear regression model for the whole data set $B_y=a\cdot B_y^i$ with the coefficient (penetration rate) $a=0.3544$. The next step is to determine the spatial dependence $a=a(x, y)$. Therefore we tested it in several spatial bins with sizes $\Delta X=5\ R_E$ and $\Delta Y=5\ R_E$. $a(x, y)$ increases towards Earth and towards midnight (Fig. 5, solid lines and diamonds) and is almost symmetrical with respect to the sign of Y GSM (not shown here). Basing on this test, the spatially resolved relation between B_y and B_y^i was defined as:

$$B_y^m=\left(a_1+a_2\cdot\left(1-\frac{|X|}{30}\right)\right)\cdot\cos\left(a_3\cdot\frac{Y}{10}\right)\cdot B_y^{\mathrm{IMF}}+a_4 \qquad (1)$$

Magnetic field values are in nT, X, Y coordinates – in R_E. The numerical coefficients were determined with the nonlinear fit. Their values with the 95% confidence ranges are: $a_1=0.3229\pm0.013$, $a_2=0.5615\pm0.039$, $a_3=0.7779\pm0.027$, $a_4=-0.0547\pm0.026$. Confidence ranges were confirmed also with the bootstrap method (e.g., Tsyganenko and Fairfield, 2004). The error for the last coefficient a_4 is quite large, but its absolute value is rather small in consistency with the standard assumption that B_y is zero, when IMF B_y is zero. The model (dotted lines in Fig. 5) fits quite well to our initial estimate.

Besides IMF, B_y was found to depend on the geodipole tilt angle τ. The tilt effect was introduced in the model as

$$B_y^{mt}=B_y^m+a_t\cdot\tau \qquad (2)$$

Here τ is in degrees and magnetic field is in nT. Coefficient of proportionality a_t was determined via the linear fit. After

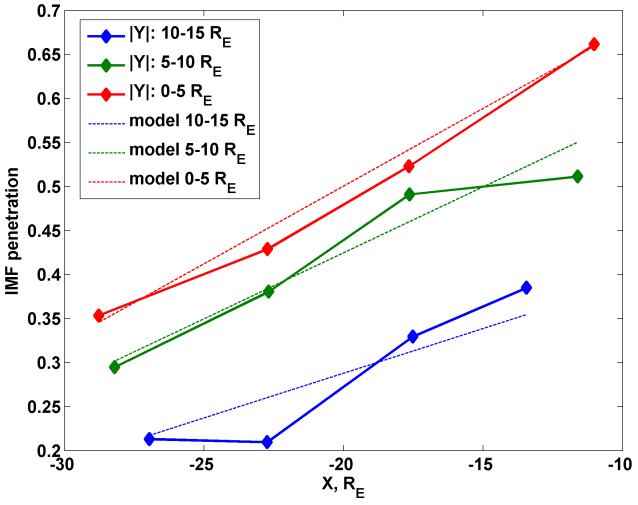

Fig. 5. Linear fit coefficients of B_y w.r.t. IMF B_y^i in several spatial bins (diamonds and solid lines). Dashed lines – the nonlinear spatial model.

a manual inspection of data, four major zones with the substantially differing tilt effect were identified in the considered plasma sheet domain (Figs. 6, 7, Table 4).

Positive B_y correlation with the tilt ($a_t>0$) appearing in Table 3 was actually limited to the pre-midnight and midnight zones. At $-31<X<-20\ R_E$ and $-5<Y<15\ R_E$ (zone "+", Fig. 7) the average addition to B_y at the maximum tilt was about 1 nT (Fig. 6a). At $X>-20\ R_E$ and in the narrower local time sector $0<Y<10\ R_E$ (zone "++", Fig. 7) the effect was four times stronger (Fig. 6a).

In the post-midnight sector the tilt dependence was almost absent (zone "0", Fig. 6). Only in its near-Earth part $X<-15\ R_E$ and $-15<Y<-5\ R_E$ (zone "−", Fig. 7) the small reverse effect of tilt appeared with average addition up to −1.5 nT (Fig. 6b). The mixed colors in Fig. 7 indicate areas, where the tilt effect was intermediate.

The tilt effect is uneven and it is difficult to describe it in a simple way. We construct a unified model only for $0<Y<10\ R_E$, where the tilt dependence on X is more uniform.

$$B_y^{mt1} = \left(a_{t1} + a_{t2}\cdot\left(1-\frac{|X|}{30}\right)\right)\cdot\cos\left(a_{t3}\cdot\frac{Y}{10}\right)\cdot B_y^{\mathrm{IMF}} + a_{t4} + \left(a_{t5} + a_{t6}\cdot\left(1-\frac{|X|}{30}\right)\right)\cdot\tau \qquad (3)$$

Values of numerical coefficients with 95% confidence ranges are: a_{t1}=0.3129±0.021, a_{t2}=0.4354±0.06, a_{t3}=0.6683±0.14, a_{t4}=−0.0816±0.047, a_{t5}=0.0252±0.038, a_{t6}=0.1869±0.01.

This model has larger error ranges due to the smaller data set. The only statistically significant difference of numerical coefficients in Eqs. (1) and (3) is between a_2 and a_{t2}.

Table 4. Regression coefficients a_t between $B_y - B_y^m$ and tilt and their 95% confidence ranges. The Zone names correspond to Fig. 7.

Zone	Selection	a_t, nT/deg	error
"-"	$-15<X<-8\ R_E$, $-15<Y<-5\ R_E$	−0.047	±0.012
"0"	$-31<X<-8\ R_E$, $-15<Y<-5\ R_E$	−0.0044	±0.002
"+"	$-31<X<-20\ R_E$, $-5<Y<15\ R_E$	0.034	±0.0026
"++"	$-20<X<-8\ R_E$, $-10<Y<0\ R_E$	0.13	±0.0064

It results in a small decrease of IMF penetration, e.g., at $X=-10\ R_E$ from 0.69 to 0.6.

The statistical quality of these models is following. The correlation coefficient of B_y and IMF B_y is 0.51, for B_y and B_y^m it is 0.54. In the zone with the maximum tilt dependence ("++", Fig. 8) the correlation of B_y and B_y^{mt} is substantially higher – 0.71. The correlation of B_y and B_y^{mt1} is 0.68.

5 Discussion

5.1 Applicability of the statistical model

The large volume of Geotail observations as well as the algorithm of the flaring removal helped to create an improved model of plasma sheet B_y with four driving parameters (IMF B_y, X, Y, τ). Inclusion of (rather flat) spatial dependence of the IMF influence results in a very modest increase of correlation coefficient, in comparison with a simplest expression $B_y \sim a\cdot B_y^i$. The major improvement is due to the geodipole tilt dependence. The model is essentially limited to the inner (high β) plasma sheet, to $-31<X<-8\ R_E$, $-15<Y<15\ R_E$ and describes the quasi-stationary configuration, since the 15-min averaging removes most of transient effects, such as flux ropes.

Our model is not in a contradiction with the previous estimates of penetration efficiency. However, Kaymaz et al. (1994b) suggested that according to IMP-8 data the penetration was somewhat higher at the flanks ($|Y|>12\ R_E$) than in the center of the magnetotail. This region is outside our domain and it is indeed reasonable to assume that IMF influence may increase at more distant flanks adjacent to LLBL.

All main features of the model were confirmed with the smaller data set $|B_x|<5$ nT (not shown here) and therefore our flaring removal procedure and criterion of the inner plasma sheet ($|B_x|<15$ nT) are reliable. Extending the model with the same technique to the outer plasma sheet and the lobe is not straightforward, since the flaring component is then larger, while B_y in question is smaller.

Our first model (Eq. 1) is the most general one and describes only the IMF influence (penetration). Though the tilt effect was not accounted for explicitly, it was effectively averaged out. Indeed the model does not depend on the sign of Y and contains data from all seasons, thus tilt effects of opposite signs are canceling each other.

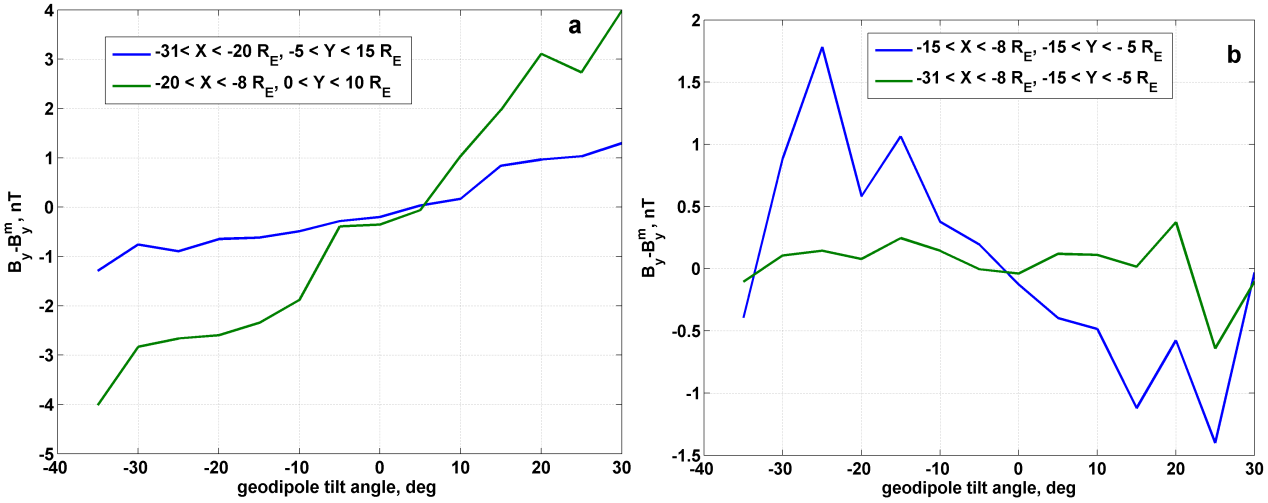

Fig. 6. Tilt angle dependence of plasma sheet B_y with subtracted IMF B_y influence. Magnetic field values are averaged in 5-deg bins of τ. **(a)** Pre-midnight and midnight sectors. **(b)** Post-midnight sector.

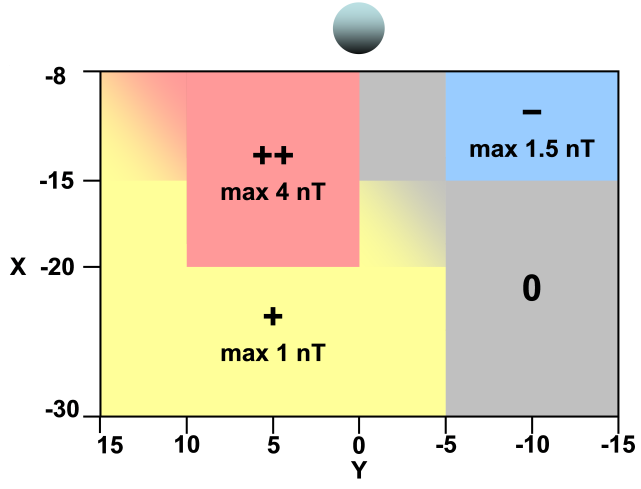

Fig. 7. The sketch of the tilt-angle effect zones. See text for details.

There exists a number of other minor factors affecting B_y. The first one to discuss is deviation of the tail axis from GSM Y due to solar wind aberration ($\sim$4°) and transient changes of solar wind direction (so-called GSM-corrected and GSW frames of reference) (e.g., Tsyganenko and Fairfield, 2004). The aberration creates the 2-R_E shift in Y coordinate at the outermost part of our tail domain. Since our model is only rather weakly sensitive to spatial coordinates, this factor is of the lesser importance.

In a tilted current sheet magnetic component along the electric current, which is important for particle dynamics, is different from B_y GSM. The tilt at the tail flanks due to the warp can reach 40° (Tsyganenko and Fairfield, 2004; Petrukovich et al., 2005). It is not quite clear however, whether the warp tilts field lines in the neutral sheet (thus affecting B_y) or it only shifts the neutral sheet surface.

The tail twist may result in a rotation of the whole tail. The twist is driven by IMF B_y and does tilt field lines. Thus plasma sheet B_y contains also a small contribution, equal to $\tan\phi \cdot B_z$, where ϕ is the twist angle. In the Tsyganenko and Fairfield (2004) model the twist angle is proportional to X, B_y^i, and in a lesser extent to B_z^i. In our data set (taking real values of B_z, X, B_z^i) the twist was generally within 10° and this contribution to B_y was equal on average to $\sim -0.1 \cdot B_y^i$. Thus the actual IMF penetration might be somewhat underestimated in our model.

Besides these factors, a more refined model should also take into account possible FAC contribution, including tilting of the FAC sheets, as well as the north-south asymmetry of flaring. Implementation of all such smaller factors in simple model similar to our's is unpractical. On the other hand they are more or less automatically accounted for in more general models like T96 or global MHD. However, the simple model might be more convenient to study specific effects.

5.2 Tilt-related asymmetry of B_y

The geodipole tilt dependence of B_y could be revealed only with the sufficiently extensive data set, covering all locations during variety of seasons. The major tilt effect is concentrated in the premidnight and midnight plasma sheet. Positive B_y-s have preference during (northern) summer season (positive tilt) while negative – during winter. Closer to Earth the effect is stronger and is larger than that of the IMF driving. The tilt effect generally disappears at the post-midnight sector but has the reverse sign in the relatively narrow near-Earth post-midnight zone. Here we present a preliminary qualitative discussion of a problem.

Some tilt effects on B_y are basically included in the T96 and T01 magnetospheric models, though it was not described explicitly. The direct point-by-point comparison of our

statistics with T96 is impossible since the difference in magnetic field could be not only due to the difference in the sources (currents), but also due to the difference in location relative to these sources. Thus we just compute the neutral sheet $B_y(Y)$ in T96 at B_x=0, X=−15 R_E, for IMF B_y^i=−5 nT, and for tilts −30°, 0°, 30° (Fig. 8). Beyond an IMF-related component (most clearly seen at the zero tilt), T96 B_y has a significant tilt-related component, positive for positive tilts and negative for negative tilts at $Y>0$. The amplitudes and the tailward extent of the tilt-induced B_y are consistent with the observations. At $Y<0$ in T96 the effect has the opposite sign, but it's magnitude is practically the same as at the dusk-side.

The source of such B_y in T96 are field-aligned currents (region 1), flowing northward and southward from the plasma sheet. At equinox a perfectly symmetric pair of FAC does not produce any B_y between them, in the plasma sheet. At non-zero tilts unequal currents generate the non-uniform B_y across the magnetotail, including some (slowly changing) net B_y in the plasma sheet. The only tilt-related modification of FAC R1 in T96 is distortion of coordinates, smoothly converting the frame in which FAC is defined (Z aligned with the dipole axis) to GSM (Tsyganenko and Stern, 1996). Then at the same X GSM the northward and southward FAC sheets have different shapes and amplitudes depending on the season. Note that initially amplitude of FAC in T96 does not depend on tilt, therefore any conductance related effects are excluded. In the later T01 model such FAC-related effects in B_y vanish well within 15 R_E (not shown here). The similar B_y profile across the magnetotail (as in Fig. 8) was also obtained from the run of BATS-R-US global MHD model, accessed via CCMC at NASA GSFC. The effect remains even if the sunlit-related conductance is switched off (not shown here).

The strong dawn-dusk asymmetry in the real data in comparison with the models could be related with the general asymmetry of the real magnetotail (e.g., ion and electron gradient drifts, thicker plasma sheet at the dawn, etc.), which at the modern level is not accounted for. Specifically it might be, e.g., due to an earlier FAC closure or to a less pronounced FAC north-south asymmetry at the dawn side. An alternative interpretation seems also reasonable: antisymmetric in Y B_y pattern within 15 R_E could be generated in accordance with the models, while the excess of the B_y-tilt effect at positive Y and further downtail might be due to some another effect.

B_y in the plasma sheet is a self-consistent reaction of the whole magnetosphere-ionosphere system and the tilt effect is just a convenient parametrization. IMF and solar wind flow impose an outer boundary condition on the magnetosphere, but local B_y is formed by a number of mechanisms, such as magnetotail convection and large-scale FAC, which in turn should match global convection and current patterns. In more detail comparison between B_y in experiment and models as well as interpretation of the effect will be accomplished in a next publication.

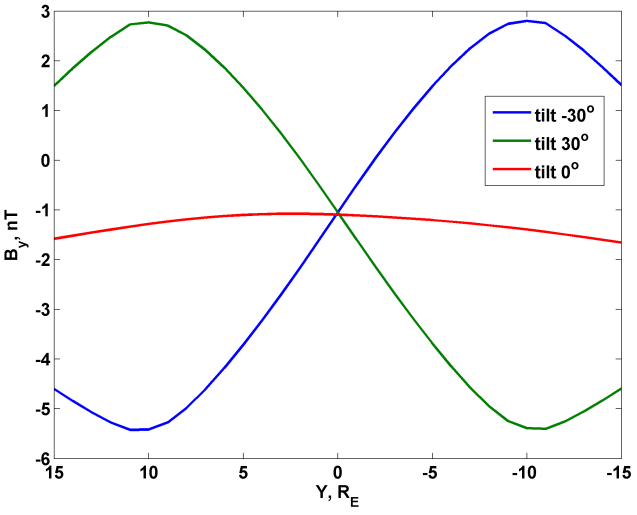

Fig. 8. T96 model field: Neutral sheet B_y at X=−15 R_E for IMF B_y^i=−5 nT and three tilt angles.

In particular the IMF B_y/season asymmetry was revealed earlier also in the polar convection. The mirror symmetry of two hemispheres with respect to IMF B_y is a well known phenomenon (the Svalgaard-Mansurov effect) (e.g., Nishida, 1978). However, Heppner and Maynard (1987) showed that convection patterns were clearer for the pair of the north polar cap and the positive IMF B_y as well as for the pair of the south polar cap and negative IMF B_y. Papitashvili et al. (2002) reported that southern summer IMF $B_y<0$ and northern summer IMF $B_y>0$ FACs were slightly larger. Finally Ruohoniemi and Greenwald (1995, 2005) explicitly formulated a "reinforcement of IMF influence" in forming convection cells at the combinations of B_y+/summer and B_y−/winter. This seasonal effect was interpreted as a result of interaction of the initially mirror-symmetric IMF B_y pattern with the day-night conductivity gradient depending on the degree of solar illumination (e.g., Tanaka, 2001) or with the single lobe cell appearing only in summer (Crooker and Rich, 1993). For an extended discussion and review of relevant studies an interested reader is referred to the papers of Tanaka (2001) and Ruohoniemi and Greenwald (2005). In the frame of our findings, such a preference might be produced by the combination of the tilt and IMF B_y effects on the FAC system.

5.3 Formation of extreme B_y

Geotail observations confirmed occurrence of extremely large B_y, reported previously by the Cluster project. The share of $|B_y|>5$ nT can reach 20–25%, while the share of $|B_y|>3$ nT − 40%. The most of such cases are not related with anomalously large IMF B_y. Our statistical model was not capable to reproduce the majority of them as well as the majority of Cluster cases (Petrukovich et al., 2007, their

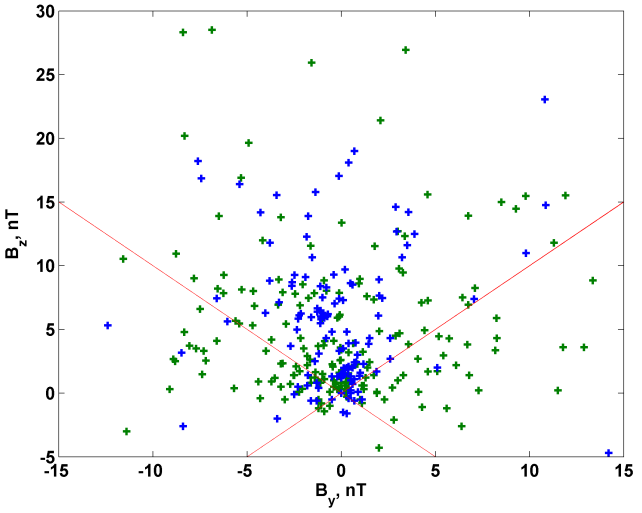

Fig. 9. Magnetic field B_y and B_z during fast current sheet crossings from Cluster 2001 and 2004 observations. (Green) – horizontal (>45°) sheets. (Blue) – only strongly tilted (>45°) sheets. Oblique lines denote $B_y=B_z$ and $B_y=-B_z$.

Table 1). Indeed, the zone $-31<X<-8\,R_E$, $0<Y<10\,R_E$ contained 671 points of $|B_y|>5$ nT, but only 125 points were reproduced by the model with the tolerance ± 2 nT. In the most of cases large B_y was substantially underestimated. Indeed in the most favorable case the IMF $B_y^i \sim 5$ nT plus the effect of maximum tilt 30° create $B_y \sim 7$ nT at $X=-15\,R_E$. With a smaller IMF and a smaller tilt it is impossible to obtain comparable values.

Since extreme B_y happen with the proper combination of tilt and IMF B_y signs, their formation may be related to the same mechanism as the statistical tilt effect. It can be due to a stronger FAC imbalance or due to amplification of existing B_y by plasma sheet convection (Hau and Erickson, 1995). Therefore the magnetospheric reaction is in each case individual and may be different in different parts of the magnetotail. In some circumstances an apparent over-reaction to IMF may occur, in other (more rare) cases IMF direction may be overridden, if the opposite sign is favored. Further advance of this problem might be achieved with better understanding of the regular tilt effect.

5.4 Role of B_y in the magnetotail

B_y creates an important asymmetry in the magnetotail and when B_y is larger than B_z, plasma dynamics may change substantially. We list and discuss just a few aspects of this problem:

1. Large B_y tilts field lines and the difference between the south and north foot-points may reach 2 h MLT (e.g., Sergeev, 1987). Indeed observations of non-conjugate auroras were often related with large IMF B_y (Stenbaek-Nielsen and Otto, 1997; Østgaard et al., 2004).

2. Non-zero B_y decreases the κ parameter, a ratio of larmor radius to minimum curvature radius, describing the degree of non-adiabaticity of particles (Büchner and Zelenyi, 1989). In particular it is often used in precipitation estimates (Newell et al., 1996). For $|B_y| \gg B_z$ the magnetic curvature radius is multiplied by $(B_y/B_z)^2$ (e.g., Shen et al., 2003). Thus for $B_y=8$ nT and $B_z=2$ nT κ may change by a factor of 16.

3. Charged particle dynamics becomes asymmetric in the north-south direction, when B_y is larger than B_z. In particular electrons and protons tend to precipitate in opposite hemispheres depending on the sign of B_y. The effect in the adiabatic approximation was described by, e.g., Sivukhin (1965), while Delcourt et al. (2000); Zhu and Parks (1993); Holland et al. (1996) performed the numerical modeling of non-adiabatic particle trajectories in a sheared current sheet.

4. New current sheet instabilities may arise in case of large B_y (Hau and Voigt, 1992). On the other hand, instabilities usually suggested for substorm onset do not include B_y, or assume that it is small.

In a particular example, strongly tilted current sheets, discovered by Cluster (Sergeev et al., 2004; Petrukovich et al., 2006; Sharma et al., 2008) were actually observed only when B_y was small. All three cases, identified by Petrukovich et al. (2006) as a slippage wave, happened with B_y less than 2 nT. The twelve intervals with the higher frequency (10 mHz) waves, identified by Zelenyi et al. (2009) as a kink drift mode, occurred with B_y less than 3 nT. A more general check was done with the full Cluster data set of fast current sheet crossings (∼360 cases during 2001 and 2004) (Runov et al., 2006). Figure 9 contains B_y and B_z values, taken in the middle of each crossing. A substantial amount of events had large B_y (larger than B_z or larger than 5 nT). However most of them belong to more horizontal sheets (with normals tilted by less than 45° from the Z GSM, shown by the green crosses). More vertical sheets (more than 45°, shown by the blue crosses) usually have B_y either within 2 nT, or smaller than B_z.

6 Conclusions

The unique Geotail data set helped to built a statistical model of plasma sheet B_y. Beyond it, observations of extremely large B_y, which is not related with the appropriately large IMF, were not rare during solar maximum and in the pre-midnight near tail, where substorms are believed to originate.

The B_y relation with the geodipole tilt is generally consistent with FAC Region 1 phenomenological structure and some previous ionospheric convection studies. However it's

specific driving mechanism remains unclear and further studies are necessary. Comparison with the global MHD simulations will be helpful. The successful model should explain also the asymmetry in Y and origin of extreme B_y. On the other hand the picture of plasma sheet B_y may give a new insight in understanding the global magnetospheric structure. Ground-based studies rarely encompass two hemispheres, while plasma sheet B_y includes integrated effect of both polar caps.

Acknowledgements. The work was supported in part by the RFBR grant 06-05-90631 and the academic exchange program. Geotail magnetic field and plasma data were provided by T. Nagai and Y. Saito through DARTS at Institute of Space and Astronautical Science, JAXA in Japan. AAP would like to thank Iku Shinohara for the help with the Geotail data access. The high resolution OMNI data set was provided by NASA GSFC. Simulation results have been provided by the Community Coordinated Modeling Center at Goddard Space Flight Center through their public Runs on Request system (http://ccmc.gsfc.nasa.gov). The CCMC is a multi-agency partnership between NASA, AFMC, AFOSR, AFRL, AFWA, NOAA, NSF and ONR. The BATS-R-US Model was developed by the Tamas Gombosi et al. at the Center for Space Environment Modeling, University of Michigan.

Topical Editor R. Nakamura thanks Z. Kaymaz and T. Pulkkinen for their help in evaluating this paper.

References

Balogh, A., Carr, C. M., Acuña, M. H., Dunlop, M. W., Beek, T. J., Brown, P., Fornacon, K.-H., Georgescu, E., Glassmeier, K.-H., Harris, J., Musmann, G., Oddy, T., and Schwingenschuh, K.: The Cluster Magnetic Field Investigation: overview of in-flight performance and initial results, Ann. Geophys., 19, 1207–1217, 2001, http://www.ann-geophys.net/19/1207/2001/.

Birn, J.: The Distortion of the Magnetotail Equilibrium Structure by a Net Cross-Tail Magnetic Field, J. Geophys. Res., 95(A6), 8019–8028, 1990.

Büchner, J., Kuznetsova, M., and Zelenyi, L. M.: Sheared field tearing instability and creation of flux ropes in the Earth magnetotail, Geophys. Res. Lett., 18, 385–388, 1991.

Büchner, J. and Zelenyi, L. M.: Regular and Chaotic Charged Particle Motion in Magnetotaillike Field Reversals, 1. Basic Theory of Trapped Motion, J. Geophys. Res., 94, 11821–11842, 1989.

Cowley, S. W. H.: Magnetospheric assymmetries associated with the y component of the IMF, Planet. Space Sci., 29, 79–96, 1981.

Cowley, S. W. H. and Hughes, W. J.: Observation of an IMF sector effect in the Y magnetic field component at geostationary orbit, Planet. Space Sci., 31, 73–90, 1983.

Crooker, N. U. and Rich, F. J.: Lobe cell convection as a summer phenomenon, J. Geophys. Res., 98, 13403–13407, 1993.

Delcourt, D. C., Zeleny, L. M., and Sauvaud, J.-A.: Magnetic moment scattering in a field reversal with nonzero B_y component, J. Geophys. Res., 105, 349–359, 2000.

Fairfield, D. H.: On the average configuration of the geomagnetic tail, J. Geophys. Res., 84, 1950–1958, 1979.

Hau, L.-N. and Voigt, G.-H.: Loss of MHD equilibrium caused by the enhancement of the magnetic B_y component in the Earth's magnetotail, J. Geophys. Res., 97, 8707–8712, 1992.

Hau, L.-N. and Erickson, G. M.: Penetration of the Interplanetary Magnetic Field By Into Earths Plasma Sheet, J. Geophys. Res., 100, 21745-21751, 1995.

Heppner, J. P. and Maynard, N. C.: Empirical High-Latitude Electric Field Models, J. Geophys. Res., 92, 4467-4489, 1987.

Holland, D. L., Chen, J., and Agranov, A.: Effects of a constant cross-tail magnetic field on the particle dynamics in the magnetotail, J. Geophys. Res., 101, 24997–25002, 1996.

Kaymaz, Z., Siscoe, G. L., Tsyganenko, N. A., and Lepping, R. P.: Magnetotail views at 33 RE: IMP 8 magnetometer observations, J. Geophys. Res., 99, 8705–8730, 1994a.

Kaymaz, Z., Siscoe, G. L., Luhmann, J. G., Lepping, R. P., and Russell, C. T.: Interplanetary magnetic field control of magnetotail magnetic field geometry: IMP 8 observations, J. Geophys. Res., 99, 11113–11126, 1994b.

Kokubun, S., Yamamoto, T., Acuna, M., Hayashi, K., Shiokawa, K., and Kawano, H.: The Geotail magnetic field experiment, J. Geomagn. Geoelectr., 46, 7–21, 1994.

Kullen, A. and Janhunen, P.: Relation of polar auroral arcs to magnetotail twisting and IMF rotation: a systematic MHD simulation study, Ann. Geophys., 22, 951–970, 2004, http://www.ann-geophys.net/22/951/2004/.

Moses, J. J., Crooker, N. U., Gorney, D. J., and Siscoe, G. L.: High-Latitude Convection on Open and Closed Field Lines for Large IMF B_y, J. Geophys. Res., 90, 11078–11082, 1985.

McComas, D. J., Russell, C. T., Elphic, R. C., and Bame, S. J.: The near-Earth cross-tail current sheet: Detailed ISEE 1 and 2 case studies, J. Geophys. Res., 91, 4287–4301, 1986.

Nakamura, R., Baumjohann, W., and Fujimoto, M.: Cluster observations of an ion-scale current sheet in the magnetotail under the presence of a guide field, J. Geophys. Res., 113, A07S16, doi:10.1029/2007/JA012760, 2008.

Newell, P. T., Feldstein, Y. I., Galperin, Y. I., and Meng, C.-I.: Morphology of nightside precipitation, J. Geophys. Res., 101, 10737–10748, 1996.

Nishida, A.: Geomagnetic diagnosis of the Magnetosphere, in: Physics and Chemistry in Space, 9, edited by: Roederer, J. G. and Wasson, J. T., Springer-Verlag, New York, 1978.

Østgaard, N., Mende, S. B., Frey, H. U., Immel, T. J., Frank, L. A., Sigwarth, J. B., and Stubbs, T. J.: Interplanetary magnetic field control of the location of substorm onset and auroral features in the conjugate hemispheres, J. Geophys. Res., 109, A07204, doi:10.1029/2003JA010370, 2004.

Papitashvili, V. O., Christiansen, F., and Neubert, T.: A new model of field-aligned currents derived from high-precision satellite magnetic field data, Geophys. Res. Lett., 29, 1683, doi:10.1029/2001GL014207, 2002.

Petrukovich, A. A., Baumjohann, W., Nakamura, R., Runov, A., and Balogh, A.: Cluster vision of the magnetotail current sheet on a macro-scale, J. Geophys. Res., 110, A06204, doi:10.1029/2004JA010825, 2005.

Petrukovich, A. A., Zhang, T. l., Baumjohann, W., Nakamura, R., Runov, A., Balogh, A., and Carr, C.: Oscillatory magnetic flux tube slippage in the plasma sheet, Ann. Geophys., 24, 1695–1704, 2006, http://www.ann-geophys.net/24/1695/2006/.

Petrukovich, A. A., Baumjohann, W., Nakamura, R., Runov, A.,

Balogh, A., and Reme, H.: Thinning and stretching of the plasma sheet, J. Geophys. Res., 112, A10213, doi:10.1029/2007JA012349, 2007.

Ruohoniemi, J. M. and Greenwald, R. A.: Observations of IMF and Seasonal Effects in High-Latitude Convection, Geophys. Res. Lett., 22, 1121–1124, 1995.

Ruohoniemi, J. M. and Greenwald, R. A.: Dependencies of high-latitude plasma convection: Consideration of interplanetary magnetic field, seasonal, and universal time factors in statistical patterns, J. Geophys. Res., 110, A09204, doi:10.1029/2004JA010815, 2005.

Runov, A., Sergeev, V. A., Nakamura, R., Baumjohann, W., Apatenkov, S., Asano, Y., Takada, T., Volwerk, M., Vrs, Z., Zhang, T. L., Sauvaud, J.-A., Rème, H., and Balogh, A.: Local structure of the magnetotail current sheet: 2001 Cluster observations, Ann. Geophys., 24, 247–262, 2006, http://www.ann-geophys.net/24/247/2006/.

Sergeev, V. A.: Penetration of the By component of the interplanetary magnetic field (IMF) into the tail of the magnetosphere, Geomag. Aerono., 27, 4–7, 1987.

Sergeev, V. A., Mitchell, D. G., Russell, C. T., and Williams, D. J.: Structure of the tail plasma/current sheet at ∼11 RE and its changes in the course of a substorm, J. Geophys. Res., 98, 17345–17366, 1993.

Sergeev, V., Runov, A., Baumjohann, W., Nakamura, R., Zhang, T. L., Balogh, A., Louarn, P., Sauvaud, J.-A., and Rème, H.: Orientation and propagation of current sheet oscillations, Geophys. Res. Lett., 31, L05807, doi:10.1029/2003GL019346, 2004.

Sharma, A. S., Nakamura, R., Runov, A., Grigorenko, E. E., Hasegawa, H., Hoshino, M., Louarn, P., Owen, C. J., Petrukovich, A., Sauvaud, J.-A., Semenov, V. S., Sergeev, V. A., Slavin, J. A., Sonnerup, B. U. Ö., Zelenyi, L. M., Fruit, G., Haaland, S., Malova, H., and Snekvik, K.: Transient and localized processes in the magnetotail: a review, Ann. Geophys., 26, 955–1006, 2008, http://www.ann-geophys.net/26/955/2008/.

Shen, C., Li, X., Dunlop, M., Liu, Z. X., Balogh, A., Baker, D. N., Hapgood, M., and Wang, X.: Analyses on the geometrical structure of magnetic field in the current sheet based on cluster measurements, J. Geophys. Res., 108, 1168, doi:10.1029/2002JA009612, 2003.

Sivukhin, D. V.: Motion of sharged particles in electromagnetic field in the drift approximation, in: Reviews of Plasma Physics, edited by: Leontovich, M. A., Consultants bureau, New York, 1, 1–104, 1965.

Stenbaek-Nielsen, H. C. and Otto, A.: Conjugate auroras and the interplanetary magnetic field, J. Geophys. Res., 102, 2223-2232, 1997.

Tanaka, T.: Interplanetary magnetic field B_y and auroral conductance effects on high-latitude ionospheric convection patterns, J. Geophys. Res., 106, 24505–24516, 2001.

Tsurutani, B. T., Jones, D. E., Lepping, R. P., Smith, E. J., and Sibeck, D. G.: The relationship between the IMF By and distant tail (150-238 Re) lobe and plasma sheet By fields, Geophys. Res. Lett., 11, 1082–1085, 1984.

Tsyganenko, N. A., Stern, D. P., and Kaymaz, Z.: Birkeland currents in the plasma sheet, J. Geophys. Res., 98, 19455–19464, 1993.

Tsyganenko, N. A. and Stern, D. P.: Modeling the global magnetic field of the large-scale Birkeland current systems, J. Geophys. Res., 101, 27187–27198, 1996.

Tsyganenko, N. A. and Fairfield, D. H.: Global shape of the magnetotail current sheet as derived from Geotail and Polar data, J. Geophys. Res., 109, A03218, doi:10.1029/2003JA010062, 2004.

Voigt, G.-H. and Hilmer, R. V.: The influence of the IMF By component on the Earth's magneto-hydrostatic magnetotail, in: Magnetotail Physics, edited by: Lui, A. T., 91, John Hopkins Univ., Baltimore, Maryland, 1987.

Watanabe, M., Sofko, G. J., Kabin, K., Rankin, R., Ridley, A. J., Clauer, C. R., and Gombosi, T. I.: Origin of the interhemispheric potential mismatch of merging cells for interplanetary magnetic field BY -dominated periods, J. Geophys. Res., 112, A10205, doi:10.1029/2006JA012179, 2007.

Wing, S., Newell, P. T., Sibeck, D. G., and Baker, K. B.: A Large Statistical Study of the Entry of Interplanetary Magnetic Field Y-Component into the Magnetosphere, Geophys. Res. Lett., 22, 2083–2086, 1995.

Zhu, Z. and Parks, G.: Particle orbits in model current sheets with a nonzero By component, J. Geophys. Res., 98, 7603–7608, 1993.

Zelenyi, L. M., Artemyev, A. V., Petrukovich, A. A., Nakamura, R., Malova, H. V., and Popov, V. Y.: Low frequency eigenmodes of thin anisotropic current sheets and Cluster observations, Ann. Geophys., 27, 861–868, 2009, http://www.ann-geophys.net/27/861/2009/.